Evolution of nanodomains during the electric-field-induced relaxor to normal ferroelectric phase transition in a Sc-doped Pb (Mg 1 3 Nb 2 3) O 3 ceramic

W. Qu, X. Zhao, and X. Tan

Citation: Journal of Applied Physics **102**, 084101 (2007); doi: 10.1063/1.2795677
View online: http://dx.doi.org/10.1063/1.2795677
View Table of Contents: http://scitation.aip.org/content/aip/journal/jap/102/8?ver=pdfcov
Published by the AIP Publishing

Evolution of nanodomains during the electric-field-induced relaxor to normal ferroelectric phase transition in a Sc-doped $Pb(Mg_{1/3}Nb_{2/3})O_3$ ceramic

W. Qu, X. Zhao, and X. Tan[a)]
Department of Materials Science and Engineering, Iowa State University, Ames, Iowa 50011, USA

(Received 11 July 2007; accepted 17 August 2007; published online 16 October 2007)

Sc doping in $Pb(Mg_{1/3}Nb_{2/3})O_3$ enhances the *B*-site 1:1 cation order significantly but promotes the ferroelectric polar order moderately. At low doping levels, the electrical polar domains remain at the nanometer scale and the relaxor ferroelectric behavior is preserved. A normal ferroelectric state can be triggered with electric fields from the relaxor state at lower temperatures. This electric-field-induced phase transition process was directly observed with an *in situ* transmission electron microscopy technique in a 4 at. % Sc-doped $Pb(Mg_{1/3}Nb_{2/3})O_3$ polycrystalline ceramic under different conditions. It was found that the phase transition started at the grain boundary and took two steps to complete: The gradual coalescence of the polar nanodomains and the abrupt formation of the long-range ferroelectric domains. During the growth of the polar nanodomains, the morphology of the cation ordered chemical domains does not change. Furthermore, these chemical domains seem to have no strong resistance to the growth of polar domains in Sc-doped $Pb(Mg_{1/3}Nb_{2/3})O_3$.
 [DOI: 10.1063/1.2795677]

I. INTRODUCTION

Relaxor ferroelectrics have been extensively studied due to their extraordinary dielectric, ferroelectric, and electrostrictive properties and accordingly their applications in multilayer capacitors, actuators, and electro-optic devices.[1] The most distinctive features of this type of ferroelectrics are the diffuse phase transition, the frequency dispersion in dielectric response, and the electric-field-induced relaxor to normal ferroelectric phase transition.[2]

$Pb(Mg_{1/3}Nb_{2/3})O_3$ (PMN) has been considered as the prototype relaxor ferroelectrics since its discovery by Smolenskii and Agranovskaya in 1958.[3] At room temperature, it has a cubic ABO_3 perovskite structure, where Pb^{2+} occupies the *A* site while Mg^{2+} and Nb^{5+} share the *B* site. The structure inevitably involves local compositional fluctuations in the distribution of the Mg and Nb cations on the *B*-site sublattice. Such fluctuations typically manifest themselves as the 1:1 cation order on the *B*-site sublattice by unit cell doubling at the nanometer scale.[4] This cation ordering was suggested to account for the diffuse phase transition and the strong frequency dispersion in dielectric permittivity.[5] Transmission electron microscopy (TEM) study by Krause *et al.*[6] and Hilton *et al.*[7] directly imaged the *B*-site cation ordered nanometer-scaled domains. The nonstoichiometric chemical ordering in PMN-based 1:2 complex perovskites is described by the "random site" model.[8] In this model, every other {111} planes of the *B*-site sublattice are occupied exclusively by Nb^{5+} while the remaining {111} planes are occupied by a random 2:1 distribution of Mg^{2+} and Nb^{5+}. The random site model has obtained direct support from the atomic resolution *Z*-contrast imaging study.[9] According to this model, there is no charge imbalance between the *B*-site 1:1 cation ordered domains and the disordered matrix. The stability of the *B*-site cation ordered domains is believed to be caused by the slow kinetics.[4] By introducing appropriate dopants, such kinetics constraints could be overcome and long-range cation ordering can be realized.[10]

The relaxor ferroelectric PMN contains electrical dipoles as well. In contrast to normal ferroelectrics, the ordered regions of these electrical dipoles are confined at the nanometer scale, forming the so-called polar nanoregions (PNRs). The PNRs persist up to the temperature T_d of Burns and Docol, which is several hundred degrees above the dielectric permittivity peak temperature T_m.[11] The origin of PNRs in relaxor ferroelectrics can also be traced back to the intrinsic chemical fluctuations and the resulting charge and strain inhomogeneity.[12,13] The PNRs have been characterized by many techniques, such as biprism refractive index measurement,[11] pair distribution function analysis,[14] as well as TEM.[15,16] In PMN, the electrical dipole ordered PNRs are structurally distorted along the ⟨111⟩ direction, and the polar vector randomly fluctuates among the eight equivalent ⟨111⟩ directions.[1,17] On cooling without electric fields, the PNRs remain less than 10 nm in size.[13,18] However, various phases can be developed in the electric-field-temperature space in PMN relaxor ferroelectrics, which correspond to various electric-field-induced phase transitions.[2]

Both the *B*-site cation ordering and the electrical dipole ordering are believed to play important roles in determining the peculiar ferroelectric behavior of PMN.[19] Therefore, observing the evolution of both the chemical and electrical domains under applied electric fields is highly expected to reveal the inter-relationship and the interactions between them. However, due to technical difficulties, there have been no publications on the direct observation of such evolution at the nanoscale with TEM until recently when we briefly reported the growth of polar nanodomains during a field-

[a)]Electronic mail: xtan@iastate.edu

cooling process.[20] In the present paper, more detailed results are reported, including the macroscopic properties measurement, the polar nanodomain growth during a poling process, the response of chemical nanodomains to applied electric fields, and the interactions of the growing polar domains with the chemical cation ordered domains.

II. EXPERIMENTAL PROCEDURE

The Sc dopant is introduced through forming a solid solution of $Pb(Mg_{1/3}Nb_{2/3})O_3$ with $Pb(Sc_{1/2}Nb_{1/2})O_3$ (PSN). The composition of the ceramic used in this study is 0.92PMN–0.08PSN (abbreviated as PSMN8 hereafter), containing 4 at. % Sc^{3+} on the *B* site. A two step solid state reaction method was employed to prepare the polycrystalline ceramic. The starting materials used in this work were commercially available and high purity (better than 99.9 wt. %) PbO, MgO, Nb_2O_5, and Sc_2O_3 powders. After vibratory milling in isopropyl alcohol for 6 h and subsequent drying, the well-mixed stoichiometric powders of *B*-site oxides were calcined at 1100 °C for 4 h. The calcined powders were then combined with PbO powder, milled for 6 h, and calcined at 900 °C for 4 h to form phase pure perovskite powder. Cold-pressing formed disks were then sintered at 1250 °C for 3 h in controlled atmosphere. At the end of sintering, a slow cooling rate of 12 °C/h to 900 °C was used to achieve long-range cation ordering in the ceramic.

The surface layers of the sintered pellets were removed and the x-ray diffraction was performed on a Siemens D500 diffractometer to check the phase purity and the cation ordering. The cation ordering was also examined by TEM dark field imaging. Then, the dielectric characterization was performed with an *LCR* meter (HP-4284A, Hewlett-Packard) in conjunction with an environmental chamber (9023, Delta Design). A heating/cooling rate of 2 °C/min was used during this measurement. Electric-field-induced phase transition was then evaluated by the thermal depolarization current measurement with a picoammeter (model 486, Keithley) and the polarization hysteresis measurement with a standardized ferroelectric test system (RT-66A, Radiant Technologies).

The *in situ* TEM experiment was carried out on a JEOL 2010 TEM operating at 200 kV with a special specimen holder. The holder has two electrical leads at the tip and a liquid nitrogen Dewar to cool the specimen to cryogenic temperatures. Detailed specimen preparation procedure for the *in situ* study can be found in previous reports.[21–23] The sample geometry is schematically shown in Fig. 1. Two half-circle shaped electrodes with their straight edges facing each other and a distance of 200 μm in between were evaporated onto the flat surface of the perforated TEM specimen with the help of a special mask. It should be noted that the presence of the central perforation disturbs the electric field. For an ideal circular perforation, it was shown that the actual field in the two small shaded areas at the edge of the central perforation in Fig. 1 is intensified and preserves the direction of the nominal field.[24] The *in situ* TEM observations in the present study were performed in the grains within these two areas and the electric field intensity specified refers to the nominal field.

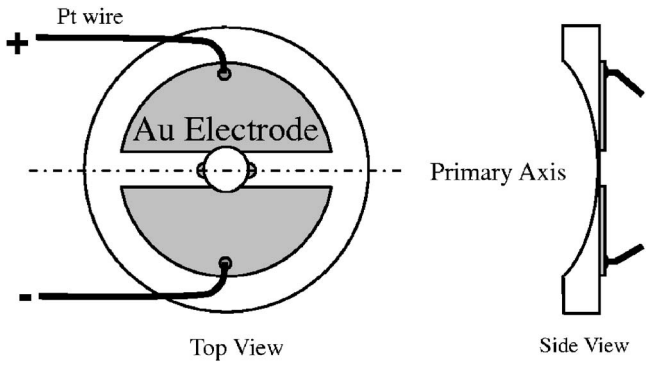

FIG. 1. Schematic diagram of the TEM specimen for the electric field *in situ* study. The specimen was fixed to the specimen holder with the nominal electric field perpendicular to the primary axis of the holder. The two dark areas at the edge of the central perforation indicate the areas where observations were made in this study.

III. RESULTS AND DISCUSSION

A. Structure and electrical properties

The x-ray diffraction pattern of the PSMN8 ceramic (cooled at 12 °C/h after sintering) is shown in Fig. 2. For comparison, the diffraction result for a pure PMN ceramic is also included. It is evident that PSMN8 still possesses a pseudocubic structure as pure PMN. The lattice parameter for PSMN8 is 4.0608 Å, increased from 4.0509 Å for the pure PMN ceramic. The increase in the unit cell size is caused by the larger ionic radius of Sc^{3+}. In addition to the major diffractions from the simple cubic perovskite structure, two extra weak peaks at ~19° and ~37°, respectively, are noticeable in the PSMN8 ceramic. These two peaks correspond to the *d*-spacing values twice those of the (111) and (311) major diffractions, respectively. The two superlattice peaks do not appear in the pure PMN ceramic. The comparison is more apparent in the inset of Fig. 2 for the $\frac{1}{2}(111)$ peak. Therefore, the x-ray diffraction results indicate a considerable enhancement of the *B*-site 1:1 cation ordering as a result of Sc doping. The introduction of larger Sc^{3+} cations (0.745 Å versus 0.72 Å of Mg^{2+}) promotes the *B*-site cation order by increasing the size difference between the cations on the two *B*-site sublattices.[25,26]

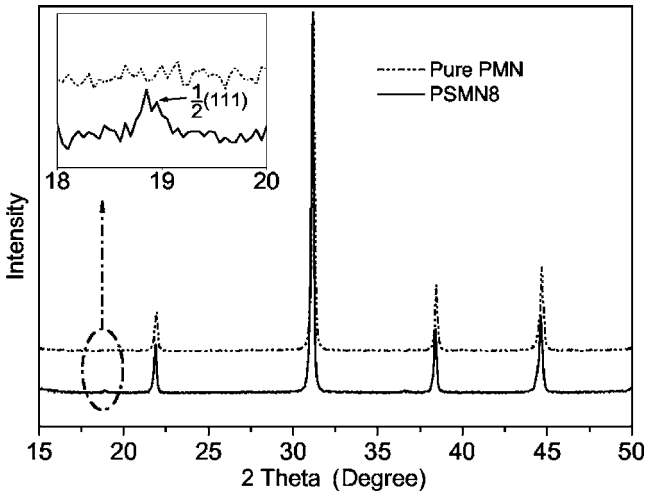

FIG. 2. X-ray diffraction spectra of the pure PMN and the PSMN8 ceramics. The inset shows a close look in the range between 18° and 20° of 2θ.

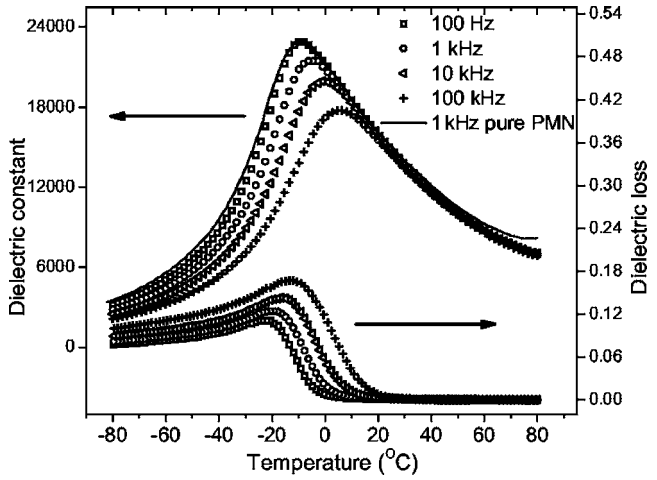

FIG. 3. Dielectric properties of the PSMN8 ceramic as a function of temperature at 100 Hz, 1 kHz, 10 kHz, and 100 kHz. The solid line shows the dielectric constant vs temperature for the pure PMN ceramic at 1 kHz.

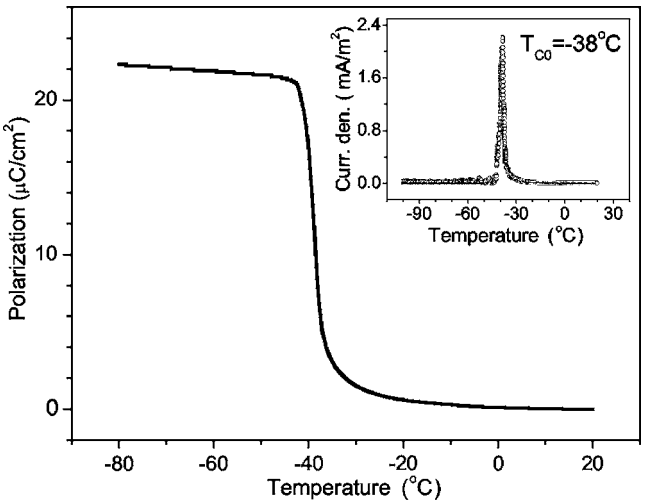

FIG. 4. Polarization of the PSMN8 ceramic obtained by integrating the depolarization current (inset) during zero-field heating after field cooling at 10 kV/cm over the measurement temperature range.

The relative dielectric permittivity as a function of temperature of PSMN8 is plotted in Fig. 3. Broad peaks and strong frequency dispersions are clearly seen, indicating that the characteristic relaxor ferroelectric behavior is still preserved after 4 at. % Sc doping. For comparison, the dielectric constant for pure PMN measured at 1 kHz is also plotted as the solid line in Fig. 3. At 1 kHz, the maximum relative permittivity ε_m was measured as 21 440 at the T_m of −5 °C for PSMN8. Compared with the T_m of −10 °C for pure PMN, Sc doping shifted the T_m slightly to a higher temperature.

For relaxor ferroelectrics, at temperatures above T_m and when $\varepsilon_m < 1.5\varepsilon$, the dielectric constant versus temperature relationship can be approximately expressed as follows:[27]

$$\frac{\varepsilon}{\varepsilon_m} = \exp\left[\frac{-(T-T_m)^2}{2\delta^2}\right], \tag{1}$$

where ε_m is the maximum dielectric constant, T_m is the temperature at which ε_m is measured, and T and ε are the temperature and the dielectric constant at this temperature, respectively. The parameter δ is the diffuseness parameter which was introduced by Smolenskii[28] to characterize the diffuse phase transition of relaxor ferroelectrics. By fitting the 1 kHz dielectric constant data to Eq. (1), the diffuseness parameter δ was determined to be 32.5 K for PSMN8 and 35.2 K for pure PMN. The lower δ in PSMN8 indicates an enhanced ferroelectric behavior after Sc doping.

Thermal depolarization measurement was carried out on a PSMN8 sample during zero-field heating after it had been cooled under an electric field of 10 kV/cm. The result is shown as the inset in Fig. 4. By integrating the depolarization current over the entire temperature range, the change of the polarization during zero-field heating is plotted in Fig. 4 as a function of temperature. The spike of depolarization current corresponds to the sudden release of the polarization developed during the initial field cooling, indicating a first order phase transition. This phase transition is believed to be the intrinsic phase transition from the induced normal ferroelectric phase to the ergodic relaxor phase. The intrinsic phase transition temperature T_{C0} was determined to be −38 °C for the PSMN8 ceramic, increased significantly from −60 °C for pure PMN. It is worthy of noting that the gap between T_m and T_{C0} is 33 °C for PSMN8 and 50 °C for pure PMN. In other words, Sc doping reduced the difference between T_m and T_{C0}. It should be pointed out that T_m and T_{C0} converge at T_C, the Curie point, in normal ferroelectrics. Therefore, the smaller temperature gap in PSMN8 also indicates an enhanced ferroelectric behavior. The enhanced ferroelectric behavior can be explained by taking into consideration the larger ionic size and higher ferroelectric activity of Sc^{3+} in comparison to Mg^{2+}.[26] When larger Sc^{3+} is introduced to the B site, the lattice is more open for Nb^{5+} to shuffle in response to external electric fields. In addition, Sc^{3+} is ferroelectrically more active than Mg^{2+}. Therefore, not only is the chemical ordering enhanced but also the electrical dipole ordering is moderately improved in the Sc-doped PMN relaxor ferroelectrics.

The electric-field-induced relaxor to normal ferroelectric phase transition was further characterized with the hysteresis loop measurement at different temperatures. In each measurement, the sample was cooled from room temperature at 2 °C/min to the desired temperature without electric fields. Then the polarization versus electric field hysteresis loop was measured at a peak field of 40 kV/cm. As shown in Fig. 5, the sample showed fully developed hysteresis loops at all the measuring temperatures (−50, −80, −100, −120, and −150 °C), indicating that a normal ferroelectric phase has been developed in PSMN8 under 40 kV/cm at these temperatures. The coercive field E_c increases as the temperature decreases. The remanent polarization P_r, however, initially increases when temperature decreases from −50 to −120 °C, then decreases at −150 °C. Such decrease in polarization indicates that electrical dipoles in some ferroelectric domains are frozen and cannot be switched anymore at −150 °C.

It was suggested that the coercive field measured under such condition in PMN-based relaxor ferroelectrics is approximately identical to the critical electric field delimiting

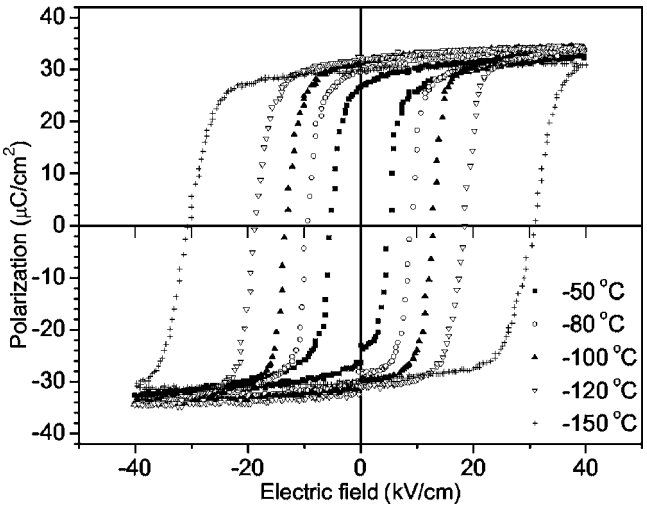

FIG. 5. Polarization vs electric field hysteresis loops measured at 4 Hz for the PSMN8 ceramic at different temperatures under a 40 kV/cm peak electric field.

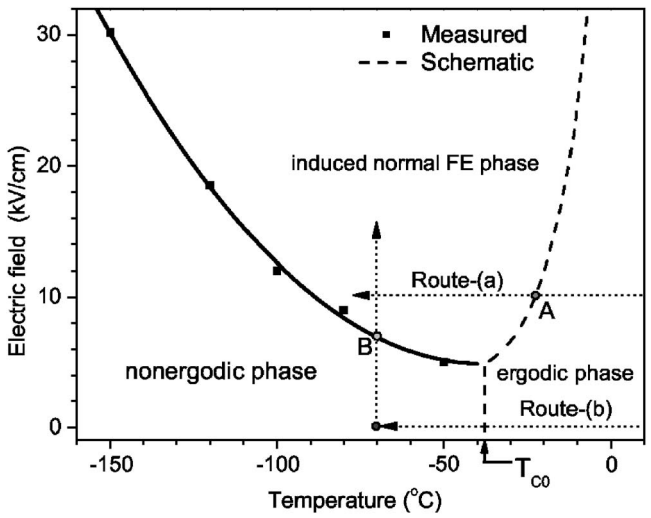

FIG. 6. *E-T* phase diagram proposed for the PSMN8 ceramic with long-range cation order. The dotted lines mark the routes used for the *in situ* TEM experiments. Route (a) represents a field-cooling process while route (b) represents a poling process at a low temperature.

the nonergodic relaxor phase from the induced normal ferroelectric phase.[2,29] Therefore, the coercive field E_c measured from Fig. 5 can be used to construct the *E-T* phase diagram of PSMN8, as shown in Fig. 6. The solid line that connects the measured E_c data points denotes the boundary between the nonergodic phase and the induced normal ferroelectric phase with switchable polarizations. The intrinsic phase transition temperature T_{C0} determined from the thermal depolarization measurement is indicated by the arrow in Fig. 6. According to Ye and Schmid,[2] there is another phase boundary which delimits the ergodic relaxor phase and the induced normal ferroelectric phase. This phase boundary is not experimentally determined in the present study and is only schematically indicated by the dashed line.

B. *In situ* TEM study

Finally, *in situ* TEM study was conducted for the PSMN8 ceramic to directly observe the electric-field-induced relaxor to normal ferroelectric phase transition at the nanometer scale. As shown in the *E-T* phase diagram in Fig. 6, the normal ferroelectric phase with switchable polarization can be developed through either a field-cooling process, route (a), or a poling process at a low temperature, route (b). In the present *in situ* TEM study, both routes were carried out.

Route (a) in Fig. 6 was followed in the *in situ* TEM study by field cooling a PSMN8 TEM specimen under a static electric field of 10 kV/cm from room temperature at 2 °C/min to predetermined temperature points. Bright field images were recorded within 5 min after temperature reached each temperature point. One grain with its ⟨110⟩ direction close to the electron beam was focused on, as shown in Fig. 7. At room temperature, very faint contrast of polar nanoregions is noticed associated with bending contours [Fig. 7(a)]. The inset shows the ⟨110⟩ zone-axis electron diffraction pattern, where the $\frac{1}{2}(111)$ superlattice diffraction spots are clearly seen. The in-plane directions ⟨001⟩ and $\langle 1\bar{1}0\rangle$ are indicated by bright arrows in Fig. 7(a). In this micrograph, the grain boundary is also noted by the bright dashed line at the top.

A fixed static electric field of 10 kV/cm, with the direction indicated by the bright arrow in Fig. 7(b), was then applied. The direction of the applied field happened to be very close to the ⟨001⟩ direction. No detectable morphological changes of the polar nanoregions were observed at room temperature under the static field. However, when temperature goes down to −50 °C, evident changes were noticed in the area close to the grain boundary, as shown in Fig. 7(b). It is clear that clustering of the polar nanoregions occurred. The coalescence of the polar nanodomains continues during the further cooling to −55 °C [Fig. 7(c)]. Until this temperature, the morphology of the nanodomains remains irregular shaped without well defined domain walls. When the temperature reaches −70 °C, a dramatic change in the domain morphology is observed [Fig. 7(d)]. Large ferroelectric domains (>200 nm) with flat domain walls close to the $\{1\bar{1}0\}$ plane appeared in close vicinity of the grain boundary. Further cooling to −90 °C leads to the growth of existing large domains and appearance of new large domains [Fig. 7(e)]. The temperature was then held constant at −90 °C. After 30 min, further growth of the large domains was noticed [Fig. 7(f)].

The results shown in Fig. 7 indicate that the field-induced relaxor to normal ferroelectric phase transition takes two stages, the gradual coalescence of polar nanodomains and the abrupt formation of long-range ferroelectric domains. This process is very similar to the one in ⟨111⟩-oriented $Pb(Mg_{1/3}Nb_{2/3})O_3$ single crystals depicted by x-ray diffraction and polarization measurement.[30,31] It should be noted that the current observation was made with an individual grain in a polycrystalline ceramic. In contrast, polarization measurements from polycrystalline ceramic samples are not able to show such a two stage process. This is where TEM can make unique contributions.

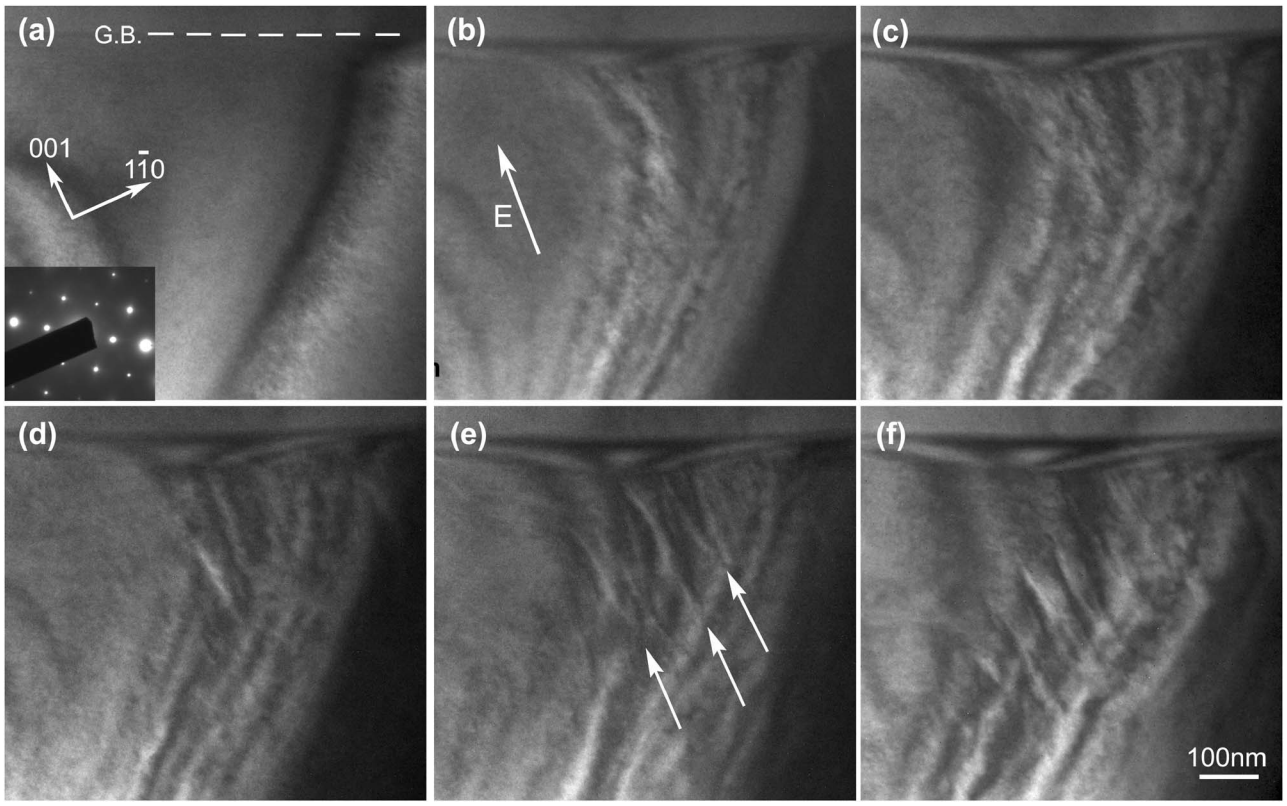

FIG. 7. The morphological evolution of the polar nanodomains during the field-cooling process under 10 kV/cm revealed by the *in situ* TEM technique. The applied field direction is shown by the arrow in (b). The tips of large ferroelectric domains are marked with bright arrows in (e). (a) The initial polar nanoregions at room temperature. The inset shows the ⟨110⟩ zone-axis selected area electron diffraction (SAED) pattern. (b) −50 °C, (c) −55 °C, (d) −70 °C, (e) −90 °C, and (f) −90 °C after 30 min.

Figure 7 also shows that the coalescence of polar nanodomains and formation of wedge-shaped domains take place in the vicinity of a grain boundary. The result is consistent with the random field model for relaxor ferroelectrics, where the polar ordering is controlled by the quenched random electric fields originating from charged point defects.[32] At grain boundaries, periodic packing of atoms is disrupted and impurity species are concentrated. This may lower the energy barrier for the alignment of local electrical dipoles at longer range. Consequently, grain boundaries are preferred sites for the initiation of the field-induced normal ferroelectric phase.

Route (b) in Fig. 6 was realized in the *in situ* TEM study by cooling another TEM specimen at 2 °C/min to −70 °C under zero electric field, then applying static electric fields up to 16 kV/cm at −70 °C. The polar domain growth during this poling process was recorded with dark field images with the ⟨100⟩ primary diffraction spot. After zero-field cooling to −70 °C, the PSMN8 ceramic preserves polar nanodomains, as shown in Fig. 8(a). A grain boundary was found at the upper right corner of the micrograph. While the temperature was maintained at −70 °C, an electric field was applied along the direction indicated by the bright arrow in Fig. 8(b). When the applied electric field was below the critical field for phase transition, coalescence of polar nanodomains occurred in the vicinity of the grain boundary. When the electric field was increased to 6 kV/cm, abrupt changes in the morphology of polar domains were observed, as shown in Fig. 8(b). Large ferroelectric domains on the order of 100 nm formed with the domain walls parallel to the {001} crystallographic planes. The tips of these large polar domains are marked with bright arrows in Fig. 8(b). This indicates that the electric-field-induced phase transition has occurred. It is noted from the *E-T* phase diagram in Fig. 6 that the critical field is ~7 kV/cm to trigger the relaxor to normal ferroelectric phase transition at −70 °C. The lower critical electric field observed in the *in situ* TEM experiment is a result of the fact that the central perforation in the TEM specimen distorts and intensifies the applied electric field. Upon further increase in electric field, a new set of domain walls appeared (with tips marked by bright arrows), replacing the existing one, as shown in Fig. 8(c). At the higher level of applied electric field [Fig. 8(c)], the new domain walls are close to the $\{1\bar{1}0\}$ plane, consistent with the observations in route (a).

The electric-field-induced normal ferroelectric phase presumably possesses a rhombohedral structure with spontaneous polarization along one of the ⟨111⟩ directions. By considering the electric field to be applied along the [100] direction, the [111] $[1\bar{1}1]$, $[11\bar{1}]$, and $[1\bar{1}\bar{1}]$ directions should be equally favored and multiple domains are expected. However, under the present experimental conditions, the direction of the applied electric fields deviates slightly from the [100] crystallographic direction. As a result, some of the ⟨111⟩ directions are favored over others. With the increasing electric field, domains with polarization directions along one of the favored ⟨111⟩ directions will grow by consuming domains

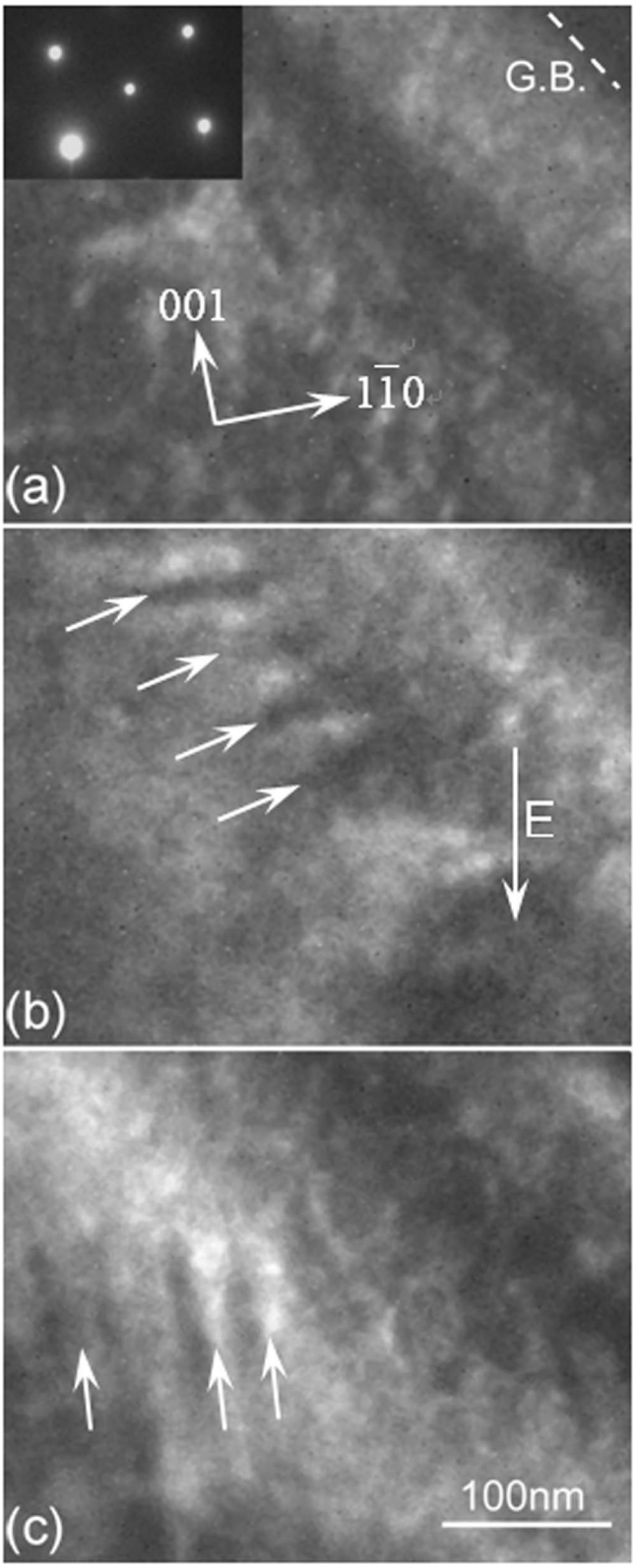

FIG. 8. The morphological evolution of the polar nanodomains during the poling process at −70 °C revealed by the *in situ* TEM technique. The applied field direction is shown by the arrow in (b). (a) 0 kV/cm at −70 °C. The inset shows the ⟨110⟩ zone-axis SAED pattern. (b) 6 kV/cm and (c) 16 kV/cm.

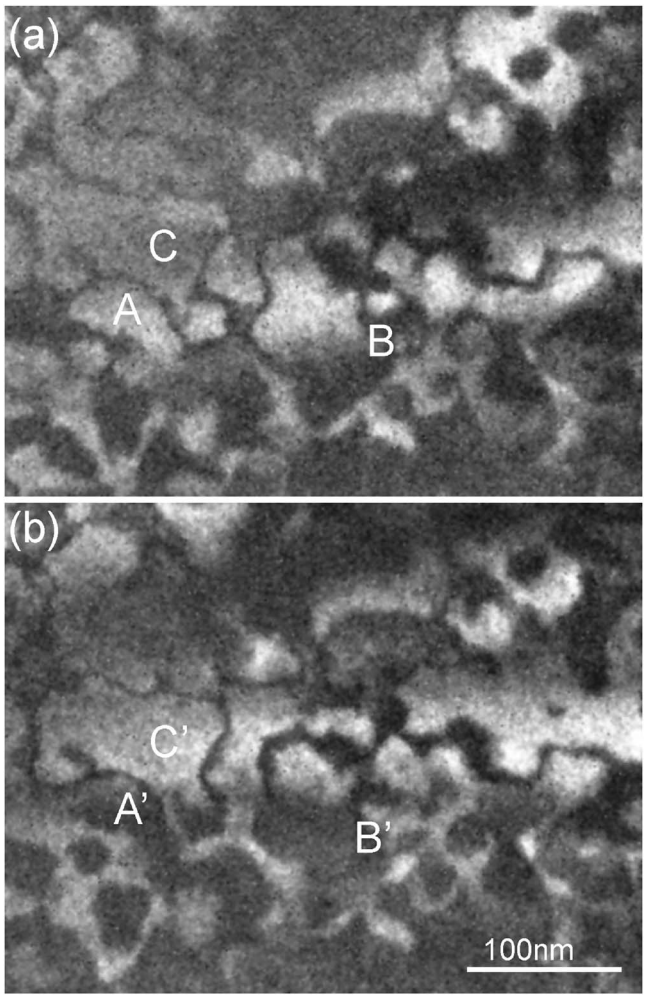

FIG. 9. The change in the contrast of the cation ordered domains in the same grain as in Fig. 7 during the field-induced relaxor to normal ferroelectric phase transition. (a) 10 kV/cm at room temperature and (b) 10 kV/cm at −65 °C.

with polarization directions along one of the disfavored ⟨111⟩ directions. The observed {1$\bar{1}$0} domain walls are therefore electrically charged. It should be pointed out here that there is an alternative interpretation of these domain walls. Close examination of Figs. 7(f) and 8(c) shows that the multiple domains may merge to a single domain as they grow. Therefore, these domain walls could possibly be the rhombohedral/pseudocubic phase boundary.

Figures 7 and 8 indicate that the field-cooling process, route (a), and the low temperature poling process, route (b), share some common features as for the relaxor to normal ferroelectric phase transition. First, the transition initiates at grain boundaries in both routes. Second, the transition takes two stages to complete during the decrease in temperature in route (a) or the increase in electric field in route (b): The gradual coalescence of polar nanodomains and the abrupt formation of micrometer-sized ferroelectric domains. Third, the domains walls are roughly along {110} planes and they are the rhombohedral/pseudocubic phase boundary at the same time.

During the field-cooling process shown in Fig. 7, cation ordered domains in the same grain were also recorded under each field level through dark field imaging with the $\frac{1}{2}${111} superlattice diffraction. The original morphology of these chemical domains at room temperature and that at −65 °C under 10 kV/cm are shown in Fig. 9. It can be seen that the

cation ordered domains in PSMN8 are on the order of 100 nm, much larger than that in pure PMN. The comparison between Figs. 9(a) and 9(b) reveals that the size and morphology of the cation ordered domains remain unchanged during the field-induced relaxor to normal ferroelectric phase transition process. However, close examination indicates that there are obvious changes in the contrast of some cation ordered domains. For example, domain A in Fig. 9(a) has a bright contrast; it changes to a dark domain A′ in Fig. 9(b). The dark domain B in Fig. 9(a) turns into a bright domain B′ in Fig. 9(b). There are also many cation ordered domains with unchanged contrast [e.g., C in Fig. 9(a) versus C′ in Fig. 9(b)].

The persistence of the morphology of cation ordered domains during the electric-field-induced relaxor to ferroelectric phase transition is anticipated because the diffusion activities of *B*-site cations are extremely limited at these low temperatures. The change in contrast of some chemical domains was not initially expected and can be explained as follows. In PMN-based complex perovskite oxides, the *B*-site cations are packed periodically on {111} planes in the ordered domains. Therefore, the cation ordered domains have four variants: $\frac{1}{2}(111)$, $\frac{1}{2}(\bar{1}11)$, $\frac{1}{2}(\bar{1}\bar{1}1)$, and $\frac{1}{2}(\bar{1}1\bar{1})$. During electron diffraction, we consider dynamical conditions which permit the double diffraction route,[33] for example,

$$\left\{\frac{\bar{1}}{2}\frac{\bar{1}}{2}\frac{1}{2}\right\}+\{110\}=\left\{\frac{1}{2}\frac{1}{2}\frac{1}{2}\right\}. \quad (2)$$

That is to say, the $\frac{1}{2}(111)$ superlattice diffraction spot used for dark field imaging could have contributions from cation ordered domain variants of both $\frac{1}{2}(111)$ and $\frac{1}{2}(\bar{1}\bar{1}1)$. Upon application of external electric fields, the double diffraction route may be modified. As a consequence, the $\frac{1}{2}(\bar{1}\bar{1}1)$ domain variant turns into a dark contrast, such as domain A in Fig. 9(a). At the same time, other domain variants, $\frac{1}{2}(\bar{1}11)$ and/or $\frac{1}{2}(\bar{1}1\bar{1})$, may become favored for double diffraction to the $\frac{1}{2}(111)$ superlattice spot. This leads to the brightening in contrast of these domains, such as domain B in Fig. 9(a). However, it needs to be clarified that these changes are only the changes in imaging conditions. There are no physical changes in the cation ordered domains under conditions in the present *in situ* TEM study.

As mentioned in the Introduction, the interactions between the cation ordered chemical domains and the growing polar domains would be of high interest. In the PSMN8 ceramic studied here, large cation ordered domains facilitate the direct observation on such interactions under electric fields. Figure 10 shows a dark field micrograph of the cation ordered domains in exactly the same area within the same grain as the micrographs shown in Fig. 7. Close comparison of Figs. 7(d) and 7(f) with Fig. 10 indicates that neither the initiation of large polar domains nor the advancement of the walls of the polar domains shows a clear correlation with the underlying cation ordered domains. In other words, the chemical domains appear not to have strong interactions with the large ferroelectric domains in the 4 at. % Sc-doped PMN ceramic.

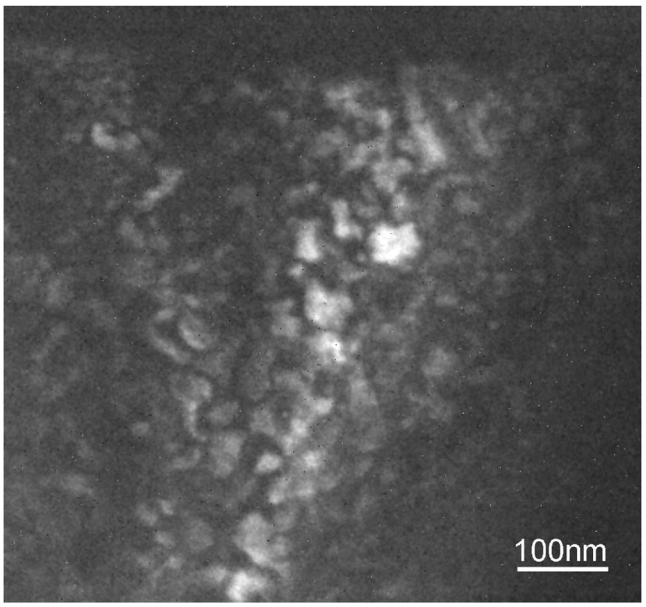

FIG. 10. Dark field imaging of the cation ordered domains in the exact same area within the same grain as those micrographs shown in Fig. 7.

IV. CONCLUSIONS

By introducing 4 at. % Sc^{3+} to the *B*-site sublattice in $Pb(Mg_{1/3}Nb_{2/3})O_3$, the pseudocubic perovskite structure and the characteristic relaxor behavior are preserved in the resulting PSMN8 ceramic. In the meantime, the *B*-site 1:1 cation order is significantly enhanced while the ferroelectric polar order is slightly promoted. Direct observation with the *in situ* TEM technique reveals that the electric-field-induced relaxor to normal ferroelectric phase transition initiates at grain boundaries. The transition involves the gradual coalescence of polar nanoregions and the successive abrupt formation of large ferroelectric domains. The formed domain/phase walls are roughly along {110} planes. The morphology of the cation ordered domains does not change under applied electric fields. Furthermore, no evidence for strong interactions of these chemical domains with the induced large ferroelectric domains is found in the Sc-doped PMN ceramic.

ACKNOWLEDGMENTS

This work was supported by the National Science Foundation through CAREER Grant No. DMR-0346819.

[1]L. E. Cross, Ferroelectrics **76**, 241 (1987).
[2]Z.-G. Ye and H. Schmid, Ferroelectrics **145**, 83 (1993).
[3]G. A. Smolenskii and A. I. Agranovskaya, Sov. Phys. Tech. Phys. **3**, 1380 (1958).
[4]M. A. Akbas and P. K. Davies, J. Am. Ceram. Soc. **80**, 2933 (1997).
[5]C. A. Randall, A. S. Bhalla, T. R. Shrout, and L. E. Cross, J. Mater. Res. **5**, 829 (1990).
[6]H. B. Krause, J. M. Cowley, and J. Wheatley, Acta Crystallogr., Sect. A: Cryst. Phys., Diffr., Theor. Gen. Crystallogr. **35**, 1015 (1979).
[7]A. D. Hilton, D. J. Barber, C. A. Randall, and T. R. Shrout, J. Mater. Sci. **25**, 3461 (1990).
[8]J. Chen, H. M. Chan, and M. P. Harmer, J. Am. Ceram. Soc. **72**, 593 (1989).
[9]Y. Yan, S. J. Pennycook, Z. Xu, and D. Viehland, Appl. Phys. Lett. **72**, 3145 (1998).
[10]X. Zhao, W. Qu, H. He, N. Vittayakorn, and X. Tan, J. Am. Ceram. Soc. **89**, 202 (2006).

[11]G. Burns and F. H. Dacol, Phys. Rev. B **28**, 2527 (1983).
[12]A. A. Bokov, JETP **84**, 994 (1997).
[13]S. Miao, J. Zhu, X. Zhang, and Z.-Y. Cheng, Phys. Rev. B **65**, 052101 (2001).
[14]I.-K. Jeong, T. W. Darling, J. K. Lee, T. Proffen, R. H. Heffner, J. S. Park, K. S. Hong, W. Dmowski, and T. Egami, Phys. Rev. Lett. **94**, 147602 (2005).
[15]M. Yoshida, S. Mori, N. Yamamoto, Y. Uesu, and J. M. Kiat, Ferroelectrics **217**, 327 (1998).
[16]R. Blinc, V. V. Laguta, B. Zalar, and J. Banys, J. Mater. Sci. **41**, 27 (2006).
[17]L. E. Cross, Ferroelectrics **151**, 305 (1994).
[18]S. Wakimoto, C. Stock, R. J. Birgeneau, Z.-G. Ye, W. Chen, W. J. L. Buyers, P. M. Gehring, and G. Shirane, Phys. Rev. B **65**, 172105 (2002).
[19]T. Mishima, H. Fujioka, S. Nagakari, K. Kamigaki, and S. Nambu, Jpn. J. Appl. Phys., Part 1 **36**, 6141 (1997).
[20]W. Qu, X. Zhao, and X. Tan, Appl. Phys. Lett. **89**, 022904 (2006).
[21]Z. Xu, X. Tan, P. Han, and J. K. Shang, Appl. Phys. Lett. **76**, 3732 (2000).
[22]H. He and X. Tan, Appl. Phys. Lett. **85**, 3187 (2004).
[23]X. Tan, H. He, and J. K. Shang, J. Mater. Res. **20**, 1641 (2005).
[24]R. M. McMeeking, ZAMP **40**, 615 (1989).
[25]P. K. Davies and M. A. Akbas, J. Phys. Chem. Solids **61**, 159 (2000).
[26]I. W. Chen, J. Phys. Chem. Solids **61**, 197 (2000).
[27]K. M. Lee, H. M. Jang, and W. J. Park, J. Mater. Res. **12**, 1603 (1997).
[28]G. A. Smolenskii, J. Phys. Soc. Jpn. **28**, 26 (1970).
[29]Z.-G. Ye, Key Eng. Mater. **155–156**, 81 (1998).
[30]S. B. Vakhrushev, J. M. Kiat, and B. Dkhil, Solid State Commun. **103**, 477 (1997).
[31]B. Dkhil and J. M. Kiat, J. Appl. Phys. **90**, 4676 (2001).
[32]V. Westphal and W. Kleemann, Phys. Rev. Lett. **68**, 847 (1992).
[33]J. Knudsen, D. I. Woodward, and I. M. Reaney, J. Mater. Res. **18**, 262 (2003).